NANO LETTERS
Letter
Cite This: Nano Lett. 2019, 19, 4380−4383
pubs.acs.org/NanoLett

Diffusion-Limited Formation of Nonequilibrium Intermetallic Nanophase for Selective Dehydrogenation

Guanghui Zhang,[†,§,#] Chenliang Ye,[‡,§,#] Wei Liu,[∥] Xiaoben Zhang,[∥] Dangsheng Su,[∥] Xin Yang,[§,⊥] Johnny Zhu Chen,[§] Zhenwei Wu,[*,§] and Jeffrey T. Miller[*,§]

[†]State Key Laboratory of Fine Chemicals, PSU-DUT Joint Center for Energy Research, School of Chemical Engineering, Dalian University of Technology, Dalian, Liaoning 116024, China

[‡]School of Chemical Engineering and Technology, Tianjin University, Tianjin 30072, China

[§]Davidson School of Chemical Engineering, Purdue University, West Lafayette, Indiana 47907, United States

[∥]Dalian National Laboratory for Clean Energy, Dalian Institute of Chemical Physics, Chinese Academy of Sciences, Dalian, Liaoning 116023, China

[⊥]School of Chemical Engineering, Huaqiao University, Xiamen, Fujian 361021, China

Supporting Information

ABSTRACT: Nonequilibrium intermetallic phases in the nanoscale were realized by diffusion-controlled solid-state transformation, forming SiO_2 supported NPs with Pd core and a CsCl type Pd_1M_1 shell, where M is Sn or Sb. The core−shell geometry is identified from scanning transmission electron microscopy and infrared spectroscopy and the crystal structure is confirmed from in situ synchrotron X-ray diffraction and X-ray absorption spectroscopy. The highly symmetric Pd_1M_1 intermetallic phase has not been reported previously and contains catalytic ensembles with high selectivity toward dehydrogenation of propane. The kinetically limited solid-state reaction is generally applicable to nanoparticle synthesis and could produce materials with desired structures and properties beyond conventional structural limits

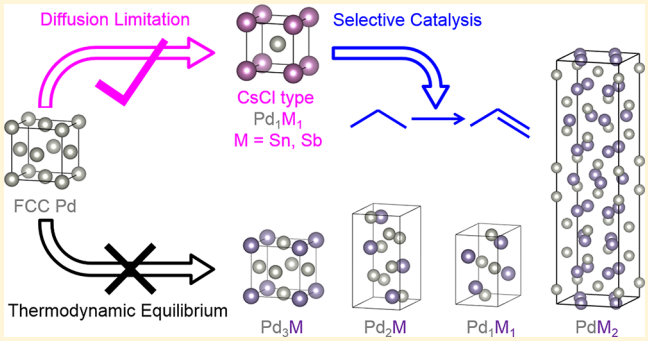

KEYWORDS: *Nonequilibrium phase, intermetallic compounds, diffusion controlled, light alkane dehydrogenation*

In the past few decades, development of functional materials has been greatly accelerated by new structures possible in the nanoscale.[1−3] For nanophases, solid-state diffusion is greatly enhanced compared to the bulk materials due to the short diffusion path and the much larger fraction of surface atoms. As a result, solid-state reactions requiring extremely high temperatures (typically above 1000 °C) for bulk materials can be realized at lower temperatures for nanomaterials,[4] where reactions are controlled by diffusion kinetics instead of thermodynamics.[5,6] Nonequilibrium phases thus become accessible, introducing new structures and interesting properties for applications in catalysis and magnetic storage.[2,7,8]

Solid-state diffusion has been recently shown to play a significant role in the formation of intermetallic nanoparticles (NPs).[2,6,9,10] For a reaction between two metals in the nanoscale, two monometallic precursors are dispersed and reduced. Because of the differences in their reduction potential, one metal is reduced first and nucleates before the second. The subsequent diffusion of the second metal into the lattice of the first metal is limited at the temperatures of reduction, often leading to partial intermetallic transformation only on the nanoparticle surface and near surface layers.[10−12] For bimetallic nanoparticles formed between Pt/Pd and Zn/In, the intermetallic shells were found to preferentially adopt crystal phases with high symmetry among all thermodynamically stable structures. Such highly symmetric phases geometrically modified the catalysts and improved their selectivity for various reactions.[9,13−15]

For different bimetallic systems, however, intermetallic phases with high symmetry are not always thermodynamically stable. Some structures, although having desired chemical properties, were not expected to form for certain bimetallic compositions according to phase diagram of bulk materials. Here we show that for Pd−Sn and Pd−Sb catalysts, diffusion-controlled solid-state reaction directs the bimetallic nanoparticles to form a nonequilibrium CsCl type Pd_1M_1 intermetallic phase at the surface. The intermetallic shells on a Pd core are stable at 550 °C and contain surface ensembles selective for catalytic dehydrogenation of propane. The finding expands the material composition horizon for nanoparticle

Received: March 9, 2019
Revised: May 6, 2019
Published: May 14, 2019

DOI: 10.1021/acs.nanolett.9b00994
Nano Lett. 2019, 19, 4380−4383

catalyst design beyond what is known according to the phase diagrams.

The Pd−Sn and Pd−Sb catalysts were prepared by reduction of the metal precursors dispersed on porous SiO_2 supports. Tin chloride or antimony chloride was first impregnated by incipient wetness, followed by a charge enhanced dry impregnation (CEDI) of tetraammine palladium nitrate.[16] During the latter step, the solution is sufficiently basified to charge the SiO_2 surface and induce strong electrostatic adsorption of positively charged Pd precursor to the deprotonated silica surface, enabling their high dispersion and subsequent formation of uniformly small Pd nanoparticles with narrow size distribution (on average 2.5 ± 0.5 nm, Figure S1). A reference Pd catalyst is prepared using the CEDI method without the addition of a second metal.

After Pd is reduced to Pd NPs, further increasing the temperature initiates partial reduction of the second metal, namely Sn or Sb, and its subsequent diffusion onto the Pd nanoparticle surface.[17] As a result, the core−shell structure could be observed by scanning transmission electron microscopy (STEM). Figure 1a shows a high-angle annular dark-field (HAADF) image of the Pd−Sn catalysts (2 wt % of Pd, 6 wt % of Sn on SiO_2). The consecutive lattice fringes in the center of the NP show that the particle has single-crystal face-centered cubic (fcc) Pd core, while relatively disordered contrast is observed around the boundary of the NP, suggesting a thinshell encapsulating the core. Carefully controlling the beam intensity as well as focusing height, we were able to minimize the amorphization induced by the beam and resolve another characteristic lattice symmetry with orthogonal spacings of 3.1 Å and 1.5 Å from the shell phase (Figure S2). Then the spatial frequencies related to the atom column distances can be separated into two typical distribution sets as filtered by 1.95 $Å^{-1}$ and 1.58 $Å^{-1}$ (Figure 1b,c), which corresponds to the characteristic diffractions of Pd (200) core and those of shell phase. It is evidenced from the distribution that the second phase dominates the nanoparticle surface whereas the metallic Pd phase composes the core. In addition, the electron dispersive X-ray spectroscopy (EDS) signal collected in the same Pd−Sn particle further confirms the aforementioned core−shell structure (Figure 1d−f, Figure S3). The Pd signal around the edge of the nanoparticle is significantly lower than that from the core, whereas the opposite is observed for Sn, confirming that the Sn locates in the surface layers of the NPs. Preferential distribution of Sb around the surface of the Pd−Sb NPs (2 wt. Pd, 6 wt. Sb on SiO_2) is also evidenced from the EDS line scan profile shown in Figure S4.

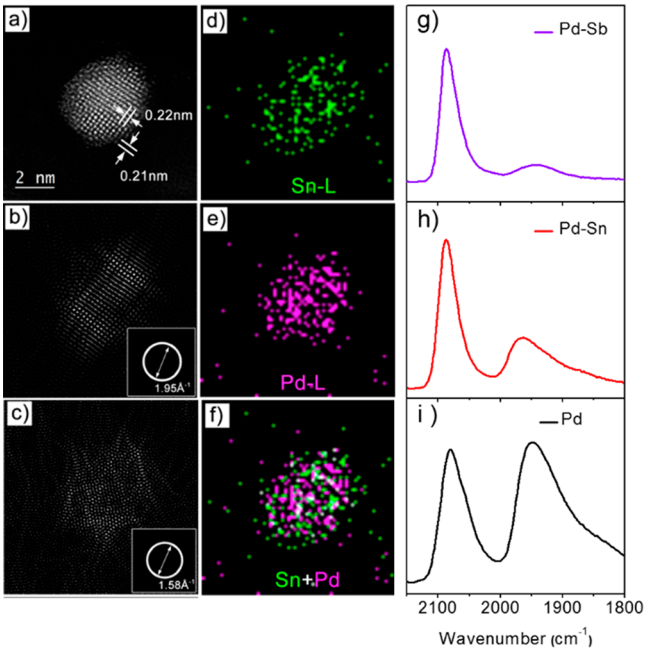

Figure 1. (a) HAADF STEM image of typical Pd−Sn particle supported on SiO_2; (b,c) the corresponding digital dark-field STEM images filtered from frequencies of 1.95 $Å^{-1}$ (Pd (200) from mainly the NP core) and 1.58 $Å^{-1}$ (a crystal plane from the Pd−Sn phase mainly on the NP shell); (d,e) the EDS elemental distribution extracted from signals of Pd-L and Sn-L edges; (f) the overlap of Pd and Sn distributions. (g−i) Infrared spectra of carbon monoxide adsorption on the Pd−Sb, Pd−Sn, and Pd catalysts

Changes of the nanoparticle shell from monometallic Pd to Pd−M bimetallic structure was further investigated by infrared spectra of carbon monoxide (CO) adsorption. As shown in Figure 1g−i, the Pd catalysts show a spectrum typical for monometallic Pd nanoparticles supported on SiO_2, where CO binds in both linear (2000−2100 cm^{-1}) and bridge fashion (1800−2000 cm^{-1}), corresponding to surface ensembles containing multiple Pd atomic neighbors.[18,19] In comparison, the Pd−Sn and Pd−Sb catalysts adsorb CO predominantly in linear fashion. The intensity of the IR peak for bridge-bound CO is significantly reduced, suggesting breaking of the Pd surface ensembles by a second metal. This indicates formation of bimetallic structures on the surface of the majority of the nanoparticles due to solid-state reactions throughout the whole supported catalyst.

The crystal structure of the bimetallic shell was studied by in situ synchrotron X-ray diffraction (sXRD). High-flux synchrotron X-ray provides enough signal intensity and resolution for diffraction from the surface layers of ∼2.5 nm NPs, while the high X-ray energy results in diffraction peaks at low 2θ angles. After background removal, the diffraction pattern of Pd/SiO_2 catalyst shows four peaks at 2.98°, 3.43°, 4.87° and 5.68° typical of an fcc lattice (Figure 2a). On the Pd−Sn and Pd−Sb catalysts (the left panel of Figure 2b), however, a new set of peaks at 3.03°, 4.28°, and 5.24° appears in addition to the fcc diffraction, corresponding to the bimetallic phase on the nanoparticle shells detected by STEM and IR. The peak positions do not match any of the known intermetallic phases recorded in the phase diagram, nor Sn, Sb or their oxides (Figure S5).[20] Instead, the relative position and intensity of the new peaks resemble that of the CsCl type Pd_1In_1 intermetallic compounds previously reported for Pd−In nanoparticle catalysts,[9] although this structure does not exist as a thermodynamically stable phase in the Pd−Sn and Pd−Sb phase diagrams.[20] To investigate the possibility that a CsCl type intermetallic phase is formed, the diffraction patterns of the two catalysts are compared with the simulated diffraction of CsCl type Pd_1M_1 intermetallics. Within this crystal symmetry, a unit cell is constructed for the simulation following the CsCl type symmetry with Sn or Sb in the corner of the cubic cell and Pd in the body center.

A lattice constant of 3.14 Å for Pd_1Sn_1 and Pd_1Sb_1 gives diffraction peaks well matching the positions of the observed peaks. When domain size is taken into consideration (the right panel of Figure 2b), a simulated pattern containing an fcc Pd phase with 1.0 nm size and a CsCl type Pd_1Sb_1 with 1.5 nm

DOI: 10.1021/acs.nanolett.9b00994
Nano Lett. 2019, 19, 4380−4383

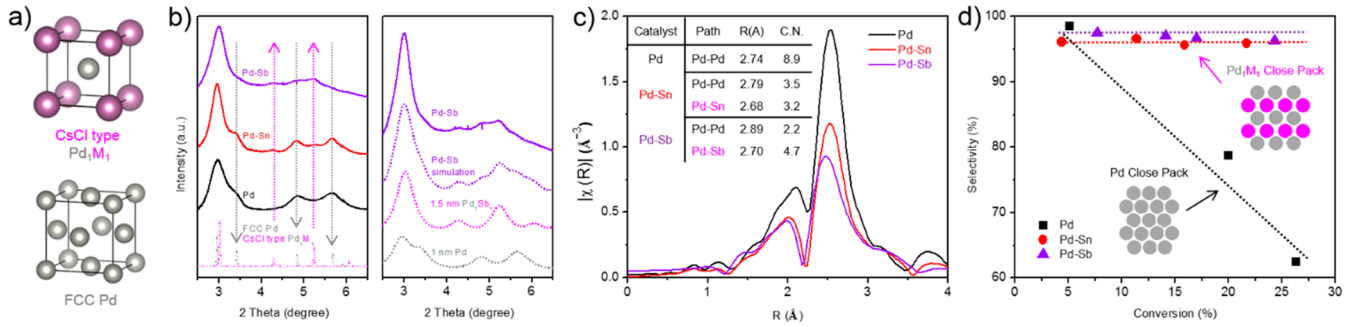

Figure 2. (a) The crystal unit cell of fcc Pd and CsCl type Pd_1M_1 intermetallics. (b) In situ sXRD patterns of the SiO_2 supported Pd, Pd−Sn, and Pd−Sb catalysts with simulated diffraction for bulk fcc Pd, Pd_1M_1, a 1.0 nm size Pd, 1.5 nm size Pd_1Sb_1, as well as their combination. (c) In situ EXAFS spectra of the Pd, Pd−Sn, and Pd−Sb catalysts and corresponding fitting results. (d) Selectivity versus conversion for propane dehydrogenation at 550 °C over Pd, Pd−Sn, and Pd−Sb catalysts and the structure of Pd (111) versus Pd_1M_1 (110) (the close pack planes).

size capture all the major features of the experimental diffraction data of the Pd−Sb catalysts, further justifying the existence of these two structures in the bimetallic NPs. In the Pd_1M_1 phase with a lattice constant of 3.14 Å, the interplanar distance of (100) is 3.14 Å, close to the 3.1 Å spacing observed in Figure S2, and the interplanar distance of (200) is 1.57 Å, consistent with the distribution set of 1.58 Å observed in STEM for the Pd−Sn catalyst. This highly symmetric CsCl type intermetallic nanostructure between Pd and Sn or Sb is not thermodynamically stable as a bulk alloy.

Varying the Sn and Sb content in the catalysts results in higher or lower intensity of the diffraction peaks coming from the bimetallic phase (Figure S6), corresponding to thicker or thinner intermetallic shells below the nanoparticle surface. The intermetallic phase forms progressively down the NP shell layers with increasing concentration of the second metal, which is consistent with a diffusion-controlled solid-state process rather than thermodynamic equilibrated reactions typically at much higher temperatures. Regardless of the Sn or Sb contents, the only alloy structure observed corresponds to the CsCl type intermetallic phase according to the diffraction patterns. The preferential formation of the CsCl structure type over the other thermodynamically stable bimetallic phases is consistent with previous reports for other intermetallic alloy catalysts. This can be explained by the lower diffusion barrier from the parent high symmetry fcc noble metal phase to this also highly symmetric structure during the kinetically limited solid-state transformation.[9]

Formation of the nonequilibrium CsCl type Pd_1Sn_1 and Pd_1Sb_1 phases is further confirmed from in situ X-ray absorption spectroscopy (XAS). Pd K edge X-ray absorption near edge spectroscopy (XANES) on the Pd−Sn and Pd−Sb catalysts (Figure S7) show that the edge energy shifts to higher values with increasing Sn and Sb contents, consistent with formation of a second bimetallic structure in increasing amount as shown by XRD. For the extended X-ray fine structure (EXAFS), the catalysts show reduced Fourier transform magnitudes compared to the monometallic Pd (Figure 2b) despite their similar particle size, indicating deconstructive interference due to a second scattering pairs. Quantitative analysis is typically challenging on bimetallic NPs where the two metals have similar atomic numbers. Nevertheless, the structural information derived from XRD previously greatly assisted the fitting analysis. The resulting bond distance is d(Pd−Sn) = 2.68 Å for the Pd−Sn catalysts and d(Pd−Sb) = 2.70 Å for the Pd−Sb catalysts, which is similar to and slightly smaller than the XRD-derived Pd—M bond distances (2.72 Å) as seen previously for other bimetallic catalysts.[10,13] The bond distances from EXAFS fittings are also consistent between samples with different Sn/Sb loadings (Figure S8, Table S1), confirming that the same intermetallic phases are formed on different samples. The Pd−Sn/Sb coordination number increases with increasing Sn/Sb loading, while the Pd−Pd coordination number decreases. The average Pd—Pd bond distances increase in the meantime due to formation of longer Pd—Pd bonds in the CsCl type Pd_1Sn_1 and Pd_1Sb_1 structure in addition to the monometallic Pd—Pd bonds in the fcc Pd core. Interestingly, the Pd_1Sn_1 and Pd_1Sb_1 phases have relatively small lattice constants and Pd—M bond distances compared to the thermodynamically stable Pd_1In_1 intermetallic compound with the same crystal symmetry. The short Pd—M bond indicates relatively strong bond strength and thus low diffusion coefficient, which likely explains why the nonequilibrium phase is only a few atomic surface layers. It is worthy to note that Sb also forms Pt_1Sb_1@Pt nanoparticles with strong Pt—Sb bonds under similar reaction conditions.[12]

The nonequilibrium Pd_1M_1 phase has atomic ensembles featuring Pd sites isolated by M on the surface (Figure 2 c) and higher edge energy (Figure S6), both of which have been previously correlated to enhanced catalytic selectivity for reactions such as light alkane dehydrogenation and semi-hydrogenation reactions.[9,13,21,22] Here the propane dehydrogenation performance of Pd−Sn/SiO_2 and Pd−Sb/SiO_2 were evaluated together with the reference Pd catalyst. While for Pd, the propylene selectivity quickly decreases from above 95% to ∼60% with increasing conversions due to side reaction propane hydrogenolysis, the two bimetallic catalysts maintain high selectivity above 95% even at high conversions, demonstrating that the diffusion directed high crystal symmetry leads to improved catalytic properties. The reaction rate per gram of Pd for the bimetallic catalysts is within one magnitude of difference compared to the monometallic Pd, similar to previous reports.[9,13] We have also attempted to compare these catalysts with Pd−Sn or Pd−Sb catalysts having solid solution structures to better demonstrate the effect of crystal phase on catalysis. However, the synthetic methods we have tried always result in diffusion-controlled solid-state reaction that prefers ordered intermetallic phases. Successful synthesis and structural confirmation of Pd−Sn and Pd−Sb solid solution NPs have not been previously reported according to our knowledge.

DOI: 10.1021/acs.nanolett.9b00994
Nano Lett. 2019, 19, 4380−4383

In conclusion, nonequilibrium intermetallic nanophases Pd_1Sn_1 and Pd_1Sb_1 were synthesized utilizing a kinetic-controlled diffusion route, which demonstrates the potential of this method to prepare nanomaterials with desired structures and properties beyond conventional structural limits.[23] The nanoparticle structures were characterized in-depth using advanced electron microscopy, in situ synchrotron X-ray methods, and infrared spectroscopy and expands the composition horizon for selective catalyst design. It rationalizes density functional theory catalyst screening on crystal structures with high symmetry (which are computation-friendly) even if they are not thermodynamically stable. Moreover, such diffusion limited solid-state reaction mechanism is generally applicable to different types of nanomaterials. The remaining unexplored nonequilibrium materials may give rise to properties not expected from the equilibrium structures and compositions and await future studies for new materials chemistry.

■ ASSOCIATED CONTENT

Supporting Information

The Supporting Information is available free of charge on the ACS Publications website at DOI: 10.1021/acs.nanolett.9b00994.

Additional information, figures, and table (PDF)

■ AUTHOR INFORMATION

Corresponding Authors

*E-mail: zhenweiwu@stanford.edu.
*E-mail: mill1194@purdue.edu.

ORCID

Guanghui Zhang: 0000-0002-5854-6909
Zhenwei Wu: 0000-0003-0400-9427
Jeffrey T. Miller: 0000-0002-6269-0620

Present Address

(Z.W.) Department of Chemical Engineering, Stanford University.

Author Contributions

#G.Z. and C.Y. contributed equally to this work

Notes

The authors declare no competing financial interest.

■ ACKNOWLEDGMENTS

This paper is based upon work supported in part by the National Science Foundation under Cooperative Agreement No. EEC-1647722. C.Y. thanks the financial support from the Chinese Scholarship Council (CSC). G.Z. acknowledges the Fundamental Research Funds for Central Universities (DUT18RC(3)057). Z.W. and J.T.M. gratefully acknowledge the financial support provided by Davidson School of Chemical Engineering, Purdue University. W.L. and D.S.S. thank the Talents Innovation Project of Dalian (2016RD04) and CAS Youth Innovation Promotion Association (2019190). Use of the Advanced Photon Source was supported by the U.S. Department of Energy, Office of Basic Energy Sciences, under contract no. DE-AC02-06CH11357. MRCAT operations, beamline 10-BM, are supported by the Department of Energy and the MRCAT member institutions. The authors also acknowledge the use of beamline 11-ID-C at APS.

■ REFERENCES

(1) Alayoglu, S.; Nilekar, A. U.; Mavrikakis, M.; Eichhorn, B. *Nat. Mater.* **2008**, *7*, 333.
(2) Bondi, J. F.; Misra, R.; Ke, X.; Sines, I. T.; Schiffer, P.; Schaak, R. E. *Chem. Mater.* **2010**, *22*, 3988−3994.
(3) Greeley, J.; Mavrikakis, M. *Nat. Mater.* **2004**, *3*, 810.
(4) Bajaj, S.; Haverty, M. G.; Arróyave, R.; Shankar, S.; et al. *Nanoscale* **2015**, *7*, 9868−9877.
(5) Rong, H.; Mao, J.; Xin, P.; He, D.; Chen, Y.; Wang, D.; Niu, Z.; Wu, Y.; Li, Y. *Adv. Mater.* **2016**, *28*, 2540−2546.
(6) Wu, L.; Fournier, A. P.; Willis, J. J.; Cargnello, M.; Tassone, C. J. *Nano Lett.* **2018**, *18*, 4053−4057.
(7) Vasquez, Y.; Luo, Z.; Schaak, R. E. *J. Am. Chem. Soc.* **2008**, *130*, 11866−11867.
(8) Nutt, M. O.; Hughes, J. B.; Wong, M. S. *Environ. Sci. Technol.* **2005**, *39*, 1346−1353.
(9) Wu, Z.; Wegener, E. C.; Tseng, H.-T.; Gallagher, J. R.; Harris, J. W.; Diaz, R. E.; Ren, Y.; Ribeiro, F. H.; Miller, J. T. *Catal. Sci. Technol.* **2016**, *6*, 6965−6976.
(10) Wu, Z.; Bukowski, B. C.; Li, Z.; Milligan, C.; Zhou, L.; Ma, T.; Wu, Y.; Ren, Y.; Ribeiro, F. H.; Delgass, W. N.; Miller, J. T.; et al. *J. Am. Chem. Soc.* **2018**, *140*, 14870−14877.
(11) Gallagher, J. R.; Childers, D. J.; Zhao, H.; Winans, R. E.; Meyer, R. J.; Miller, J. T. *Phys. Chem. Chem. Phys.* **2015**, *17* (42), 28144−28153.
(12) Ye, C.; Wu, Z.; Liu, W.; Ren, Y.; Zhang, G.; Miller, J. T. *Chem. Mater.* **2018**, *30*, 4503−4507.
(13) Childers, D. J.; Schweitzer, N. M.; Shahari, S. M. K.; Rioux, R. M.; Miller, J. T.; Meyer, R. J. *J. Catal.* **2014**, *318*, 75−84.
(14) Cybulskis, V. J.; Bukowski, B. C.; Tseng, H.-T.; Gallagher, J. R.; Wu, Z.; Wegener, E.; Kropf, A. J.; Ravel, B.; Ribeiro, F. H.; Greeley, J.; Miller, J. T. *ACS Catal.* **2017**, *7*, 4173−4181.
(15) Wegener, E. C.; Wu, Z.; Tseng, H.-T.; Gallagher, J. R.; Ren, Y.; Diaz, R. E.; Ribeiro, F. H.; Miller, J. T. *Catal. Today* **2018**, *299*, 146−153.
(16) Mehrabadi, B. A.; Eskandari, S.; Khan, U.; White, R. D.; Regalbuto, J. R. *A Review of Preparation Methods for Supported Metal Catalysts*. Elsevier, 2017; Vol. *61*, pp 1−35.
(17) Niu, Y.; Liu, X.; Wang, Y.; Zhou, S.; Lv, Z.; Zhang, L.; Shi, W.; Li, Y.; Zhang, W.; Zhang, B.; et al. *Angew. Chem., Int. Ed.* **2019**, *58*, 4232−4237.
(18) Lear, T.; Marshall, R.; Antonio Lopez-Sanchez, J.; Jackson, S. D.; Klapötke, T. M.; Bäumer, M.; Rupprechter, G.; Freund, H.-J.; Lennon, D. *J. Chem. Phys.* **2005**, *123*, 174706.
(19) Lu, J.; Fu, B.; Kung, M. C.; Xiao, G.; Elam, J. W.; Kung, H. H.; Stair, P. C. *Science* **2012**, *335*, 1205−1208.
(20) Okamoto, H. *Phase diagrams for binary alloys. Desk Handbook*; ASM International: Materials Park, OH, 2000.
(21) Tew, M. W.; Emerich, H.; van Bokhoven, J. A. *J. Phys. Chem. C* **2011**, *115*, 8457−8465.
(22) Sattler, J. J.; Ruiz-Martinez, J.; Santillan-Jimenez, E.; Weckhuysen, B. M. *Chem. Rev.* **2014**, *114*, 10613−10653.
(23) ZhuChen, J.; Wu, Z.; Zhang, X.; Choi, S.; Xiao, Y.; Varma, A.; Liu, W.; Zhang, G.; Miller, J. T. *Catal. Sci. Technol.* **2019**, *9*, 1349−1356.

DOI: 10.1021/acs.nanolett.9b00994
Nano Lett. 2019, 19, 4380−4383